Discrete CMC surfaces for doubly-curved building envelopes

Xavier Tellier, Laurent Hauswirth, Cyril Douthe, Olivier Baverel

AAG2018

Advances in Architectural Geometry 2018
Chalmers University of Technology
Gothenburg, Sweden
22-25 September 2018

www.architecturalgeometry.org/aag18

Discrete CMC surfaces for doubly-curved building envelopes

Xavier TELLIER* [a b], Laurent HAUSWIRTH[b], Cyril DOUTHE[a], Olivier BAVEREL[a c]

* [a] Laboratoire Navier UMR8205, Ecole des Ponts, IFSTTAR, CNRS
77455 Champs-sur-Marne - MLV Cedex 2
xavier.tellier@enpc.fr
[b] Université Paris-Est, Laboratoire d'Analyse et de Mathématiques Appliquées
[c] GSA / ENS Architecture Grenoble

Abstract

Constant mean curvature surfaces (CMCs) have many interesting properties for use as a form for doubly curved structural envelopes. The discretization of these surfaces has been a focus of research amongst the discrete differential geometry community. Many of the proposed discretizations have remarkable properties for envelope rationalization purposes. However, little attention has been paid to generation methods intended for designers.

This paper proposes an extension to CMCs of the method developed by Bobenko, Hoffmann and Springborn (2006) to generate minimal S-isothermic nets. The method takes as input a CMC (smooth or finely triangulated), remeshes its Gauss map with quadrangular faces, and rebuilds a CMC mesh via a parallel transformation. The resulting mesh is S-CMC, a geometric structure discovered by Hoffmann (2010). This type of mesh have planar quads and offset properties, which are of particular interest in the fabrication of gridshells.

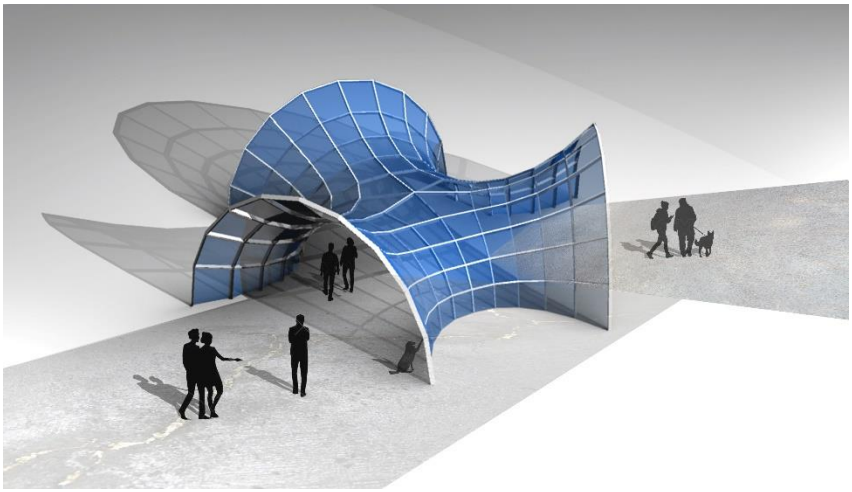

Figure 1: A steel-glass gridshell with geometry based on an S-CMC trinoid

1 Introduction

1.1 Constant mean curvature surfaces for architecture

CMCs are defined mathematically as surfaces whose mean curvature is constant. The mean curvature of a surface at a given point is the average of the maximum and the minimum principal curvatures. Some CMCs can be easily created: any soap film or bubble in static equilibrium takes the shape of a CMC. However, the family of CMCs also contains surfaces that could theoretically take the form of a bubble, but that are too unstable to exist. CMCs have other unique properties, including the fact that they solve the Plateau problem: CMCs are the surfaces with minimal area fitting a given boundary and englobing a given volume.

CMCs are particularly interesting for the design of building envelopes for the following reasons:

- They can be fitted on any boundary. This property is interesting for applications such as covering courtyards.
- They are aesthetically pleasing, as they take the harmonious shape of an inflated soap bubble.
- Rogers and Schief (2003) showed that under normal pressure, principal stress directions in CMC membranes are aligned with directions of curvature. Curvature directions are preferred directions to lay beams in a gridshell: they minimize panel curvature and node torsion, and also have offset properties. Therefore, on CMCs, curvature lines combine mechanical performance with fabrication advantages.

Minimal surfaces are the most well-known CMCs. They are a special subclass of CMC surfaces for which the mean curvature is null. They can be easily generated with a physical model (e.g. a soap film), or a numerical model (the input then being a boundary curve). However, because of their null mean curvature and due to the estimate of curvature for a stable minimal disk (Schoen 1983), they tend to be flat at their center. They thus require a boundary with a high variation of height in order to be interesting aesthetically, mechanically, and functionally. Allowing the mean curvature to be different from zero significantly broadens the spectrum of possible shapes: minimal surfaces can be ‘’inflated’’ – as can be seen in Figure 2.

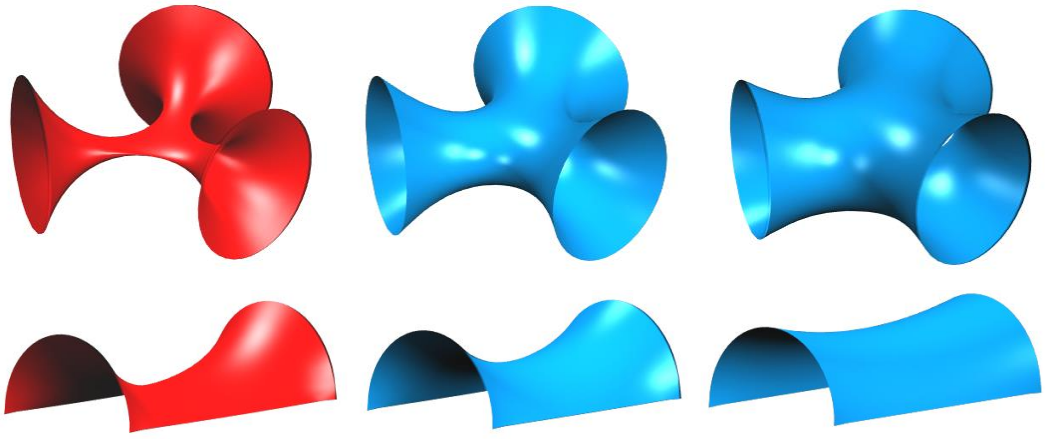

Figure 2: Comparison of minimal surfaces (left) and non-minimal CMCs (middle and right) with the same boundary. Pictures generated with Kangaroo2.

In architecture, CMCs have been used frequently in the work of Frei Otto. The most famous example is the Munich Olympic stadium, whose cable net describe a minimal surface. Other examples include membrane envelopes and inflatable structures, such as the Unite Pneu or the Airhall of Expo64. Despite the interest for smooth CMCs, the potential of discrete CMCs for building envelopes has not yet been exploited.

1.2 Related work

We will first briefly review previous work on the physical form exploration of CMCs. We will then review literature on discrete CMC surfaces relevant for the current paper. Amongst this literature, two approaches are of interest for this study: methods enabling generation of a CMC meshes on a given boundary, and one discretization of the notion of CMC, called S-CMC, which offers interesting properties for gridshell fabrication.

Form potential of CMCs

The shape of a soap film in static equilibrium is a CMC surface. This is due to the fact that a soap film has no bending stiffness and its membrane tension is uniform and isotropic. The mean curvature of a film is directly proportional to the difference of pressure between the two sides of the film.

Bach, Burkhard and Otto (1988) performed a vast exploration program of the shape potential of soap films at the IL in Stuttgart. They tested several types of film support: frames, ropes, friction-free surfaces, and even other soap films. Each type of support has a different flow of forces and yield different forms. They also explored the effect of difference of pressure between the two sides of a film. Their work revealed the ability of CMCs to fit boundaries with holes and thus assume complex topologies. Trying to fit the same boundaries with traditional methods such as NURBS surfaces would be highly tedious. Inspired by their work, Figure 3 shows a soap bubble whose boundary is a model of the British Museum atrium.

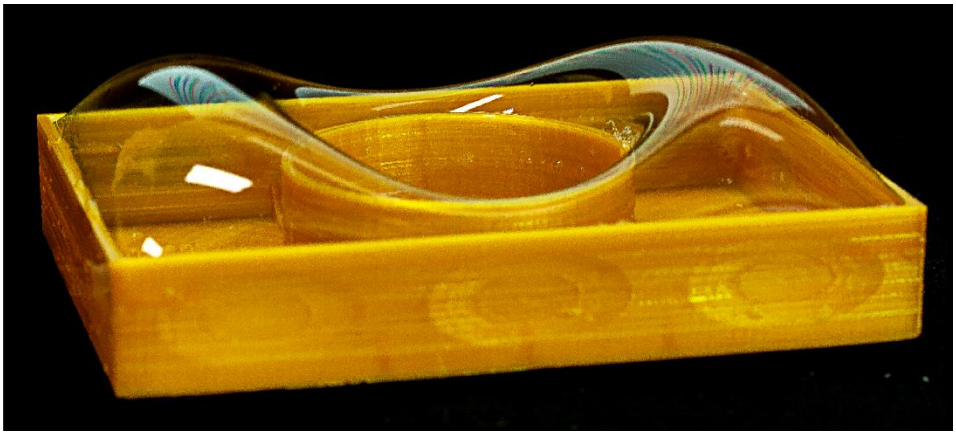

Figure 3 : A soap bubble on a boundary similar to the one of the atrium of the British Museum

Generation of triangular CMC mesh by searching critical points of a functional

Many methods have been developed to generate a triangular mesh with minimal area under a volume constraint. One well-known software implementing such a method is Surface Evolver, developed by Brakke (1992). Oberknappl and Polhier (1999) generate minimal surfaces in S^3 by minimizing an area functional. They then transform them into CMCs in R^3 using the Lawson correspondence, which has been recently generalized in the discrete case by Bobenko and Romon (2017). In order to improve the robustness of CMC mesh generation, Pan *et al* (2012) propose to look for critical points of an energy based on a Centroidal Voronoi Tessellation rather than minimizing the area. For designers, one of the most accessible tools to generate CMCs is the plugin Kangaroo2 for Grasshopper, which is based on the algorithm developed by Bouaziz *et al* (2012) to handle various geometric constraints.

S-CMC meshes

Smooth CMCs have the property of being parametrized along curvature lines by isothermic coordinates. Bobenko and Hoffmann (2016) propose a discretization of this property with S-isothermic

meshes. A subclass of this family (referred to as type 1), have the particularity of having an inscribed circle in each face, and sphere associated with each summit – two spheres being tangent if the corresponding nodes share an edge. Bobenko, Hoffmann and Springborn (2006) developed a theory of minimal S-isothermic meshes based on this structure. Numerous discrete minimal surfaces were then constructed by Bücking (2007).

Hertrich-Jeromin and Pedit (1996) show that smooth CMCs are characterized by the fact that their Christoffel dual is also a Darboux transform of the surface. Hoffmann (2010) proposes a discretization of this property for S-isothermic meshes of type 1. Meshes fulfilling this property are called S-CMCs.

S-CMC surfaces have geometric properties which are of particular interest for fabrication purposes. Firstly, they are quad meshes with planar faces and torsion-free nodes. This property significantly eases the fabrication of a structure such as a gridshell. Secondly, they admit an offset in which some edges are located at constant distance h_1 from the mesh, and the other edges are located at a distance h_2. This property enables a perfect alignment of the beams at the node while using only two different beam cross sections, as illustrated in Figure 4. We will use the term *orthotropic edge offsets* to refer to this kind of offset. Thirdly, each face has an inscribed circle. As a result, faces are « roughly square », which provides aesthetic value to the mesh, and also minimizes material loss if panels are cut out of a larger sheet. Finally, S-CMC meshes have interesting mechanical properties. They are close to a smooth CMC, which is funicular under a uniform pressure loading. Furthermore, since the mesh approximates the curvature lines of the smooth CMC, the orientation of the edges is optimized for beams to resist such a load (Rogers and Schief, 2003).

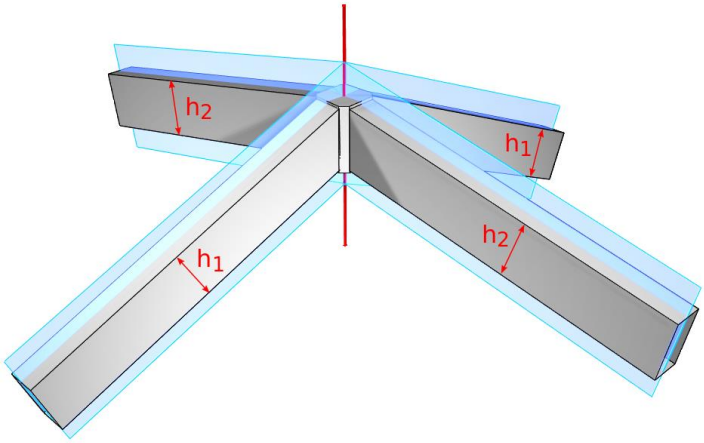

Figure 4: A torsion free node in an orthotropic edge offset mesh

1.3 Contribution and overview

In this paper, we propose a method to generate quadrangular S-CMC meshes and a structure that allows a change of curvature sign. In Section 2, we present an overview of the method. Section 3 describes how smooth or finely triangulated CMCs can be generated. Section 4 explains how the Gauss map of the smooth CMC can be discretized. The construction of a discrete S-CMC surface from this Gauss map is detailed in Section 5. In Section 6, we explain how the work presented in Sections 3 and 4 must be modified in areas with a change of curvature sign. Finally, in Section 7, we give some examples of S-CMC surfaces and discuss the use of the method in practice.

2 Overview of the method

The workflow is similar to the one used by Bobenko, Hoffmann and Springborn (2006) to generate minimal meshes. The process consists of four steps, which are shown in Figure 5.

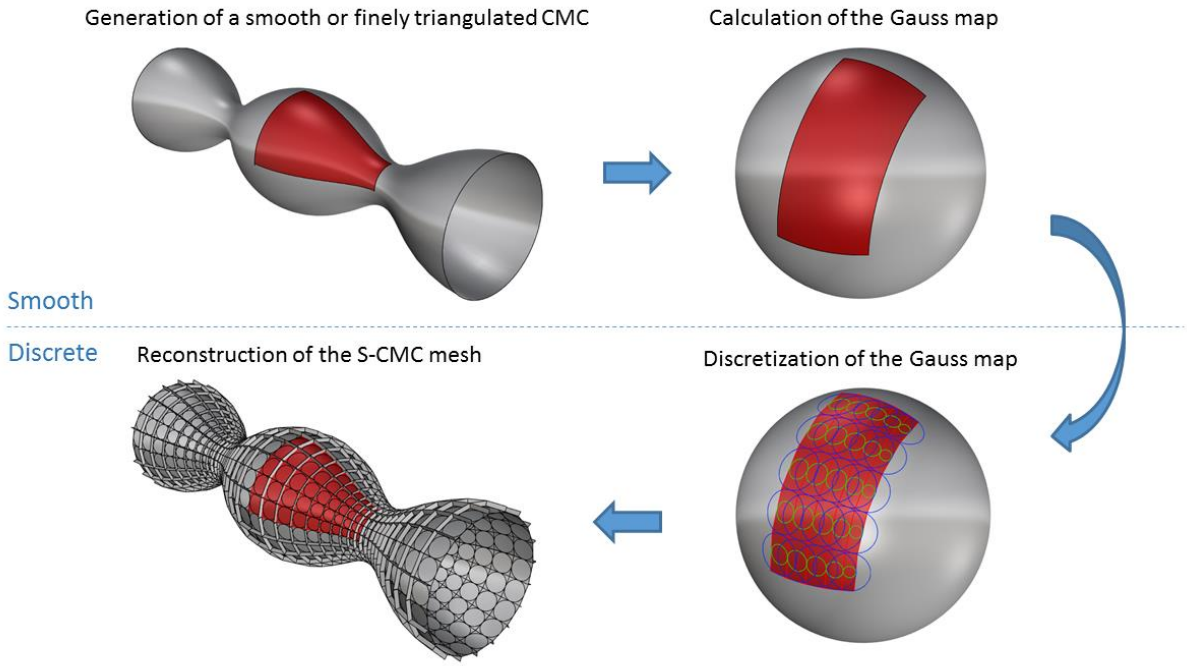

Figure 5: Overview of the discretization method

In the first step, a CMC surface – smooth or triangulated – is generated. An isothermic network of curvature lines is generated. In the second step, the Gauss map of the surface is calculated. The boundary of the Gauss map and the topology of the curvature lines are used to generate a discrete Gauss map in the third step. Finally, in the fourth step, the Gauss map is transformed into an S-CMC mesh by a parallel transformation.

3 Generation of input smooth CMCs

In this section, we shall present how we generate smooth CMC surfaces for use as an input in our algorithm.

CMC generation

For the first step of our process, smooth or finely triangulated CMCs are generated. The former option is used when an analytical equations is known for the surface. An example is the unduloid, shown in Figure 5. When no analytical equation is available, a CMC triangular mesh is generated by using the functions « SoapFilm » and « Volume » of the software Kangaroo2. CMC surfaces shown in Figure 2 are generated by this method.

Isothermic orthogonal net

An isothermic network of curvature lines is then drawn on the surface. The isothermic property means that each face is "square", this is necessary for the net to be approximated by an S-CMC mesh. This part is performed in the CAD software Rhino. For smooth surfaces, a code was developed for this purpose using the geometry functions of RhinoScriptSyntax. For triangulated surfaces obtained by Kangaroo2, a network of curvature lines is drawn using the software EvoluteTools T.MAP. Singularities of the network shall be located on the umbilical points of the surface. The order of these umbilical points is a multiple of ½ (Gutierrez and Sotomayor 1986), so the singularities have an even valence: singularities of valence 3, 5 and 7 are not possible since they correspond to umbilics of order ¼, -¼, and -¾ respectively. There are exceptions of course if a singularity is located on the mesh boundary.

Gauss map

The Gauss map of the surface is then computed. For analytical surfaces, the exact normal is computed. For triangulated surfaces, the direction of the normal at a given vertex is computed as the gradient of the area of the adjacent faces.

4 Discretization of the Gauss map

The discretization of the Gauss map is done by generating an orthogonal double circle packing (ODCP) on the unit sphere with a boundary close to the one of the smooth Gauss map. The geometric structure of ODCP is explained in Section 4.1 and the generation method in Section 4.2. The transformation of the ODCP into a discrete Gauss map is described in Section 4.3. The rich structure of this discrete CMC Gauss map – which allows generation by an ODCP – was developed by Hoffmann (2010).

4.1 Orthogonal double circle packings

An *orthogonal double-circle packing* (ODCP) in the plane consists of pairs of circles, where two circles of a given pair are concentric. Such a structure is shown in Figure 6. The packing can be decomposed into two families, represented by red and blue. Having in mind the construction of the Gauss map, one family will be called the *node-centered circles* (in red), and the other one the *inscribed circles* (in blue). For each family, the smaller circles are tangent in one direction, and the larger circles in the other one.

When a pair of circles from each family intersect, they fulfill the following rule: the smaller circle of one pair intersects orthogonally the larger circle of the other pair. This property is shown in Figure 7. Thanks to this rule, a quad mesh can be drawn between the node-centered circles, and the inscribed circles (in blue) are then tangent to the edges of this mesh.

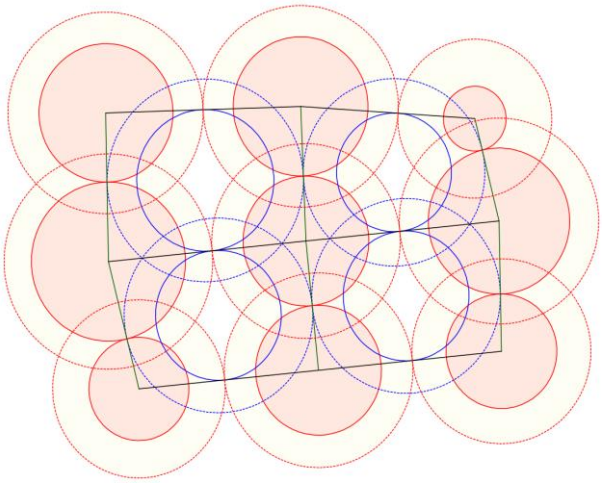

Figure 6: Orthogonal double-circle packing (ODCP)

In order to generate the Gauss map, ODCP will be generated on S^2, the unit sphere. The rules described above are applied in the same way as in the plane, except that straight lines are replaced by arcs of great circles.

4.2 Generation of an ODCP

In this section, we show how an ODCP can be generated with given combinatorics and boundary angles. In a first step, radii of circles compatible with the ODCP structure and the boundary conditions are found using a Newton algorithm. The compatibility of the circles can be expressed by two sets of constraints. In a second step, the ODCP is constructed using the radii and the orthogonal properties.

First Constraint on radii: orthogonal intersection

The orthogonality condition between two secant pairs of circles yields one constraint per pair of circles. As shown in Figure 7, let r_0 and R_0 be the spherical radii of one pair of circles, and r_1 and R_1 the radii of the second one. The geodesic distance d between the centers of the two pairs can be calculated by the spherical cosine rule:

$$\cos(d) = \cos(r_0)\cos(R_1)$$
$$\cos(d) = \cos(R_0)\cos(r_1)$$

Assuming that all circles have a radius lower than $\pi/2$, and thus a non-null cosine, we obtain the following relation:

$$\frac{\cos(r_0)}{\cos(R_0)} = \frac{\cos(r_1)}{\cos(R_1)}$$

Since this relation must hold for all intersecting pairs of circles, the cosine ratio must be identical for all pairs of circles:

$$\frac{\cos(r)}{\cos(R)} = t = cte \geq 1 \qquad (1)$$

The constant *t* will play an important role in the structure of the offset, as will be shown in Section 4.3.

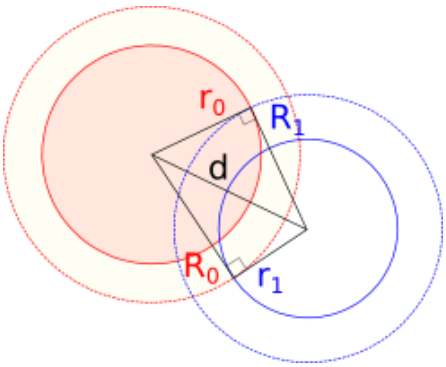

Figure 7: Two secant pairs of circle of an ODCP

Second constraint on radii: closure of mesh faces

The second set of constraints concerns how all the neighboring circles of a given circle close around it.

Bobenko *et al* (2006) showed that the Napier formula for a right spherical triangle can be expressed as follows:

$$\varphi = \arctan(e^{\gamma_2-\gamma_1}) + \arctan(e^{\gamma_2+\gamma_1})$$

in which $\gamma_i = \ln(\tan\frac{r_i}{2})$ and r_1, r_2 and φ are shown in Figure 8 :

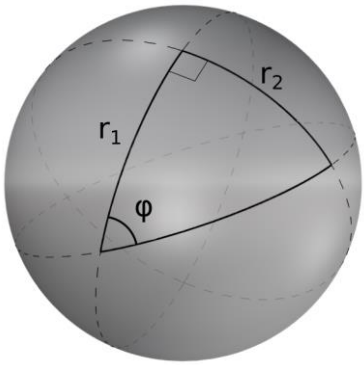

Figure 8: Napier rule for a right spherical triangle

Since circles intersect orthogonally, the Napier formula can be used to compute all the angles centered at a point M, as shown in Figure 9:

$$\varphi_k = \arctan\left(e^{\Gamma_k - \gamma_i}\right) + \arctan\left(e^{\Gamma_k + \gamma_i}\right)$$

$$\psi_k = \arctan\left(e^{\gamma_k - \Gamma_i}\right) + \arctan\left(e^{\gamma_k + \Gamma_i}\right)$$

Where $\gamma_i = \ln\left(tan\frac{r_i}{2}\right)$; $\Gamma_i = \ln\left(tan\frac{R_i}{2}\right)$; $\varphi_k = \widehat{A_k M P_k}$ and $\psi_k = \widehat{P_k M B_k}$

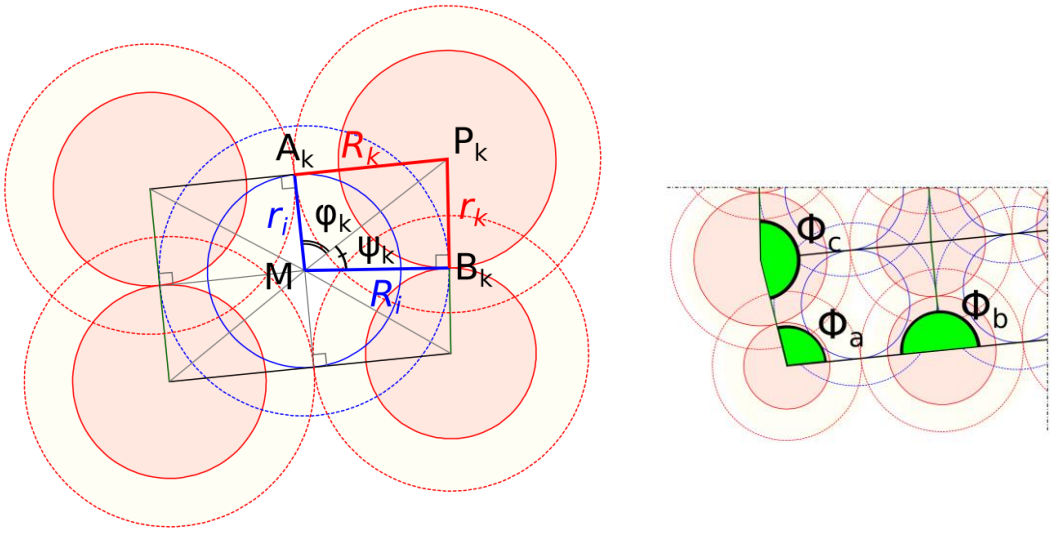

Figure 9: Angles around the center of a circle (left) and boundary angles Φ (right)

For a pair of circles not located on the boundary, the angles must add up to 2π:

$$\sum_{k=1}^{n} (\varphi_k + \psi_k) = 2\pi \qquad (2a)$$

For pairs located on the boundary, the sum of the angles around a point is a boundary angle Φ that needs to be calculated from the smooth Gauss map, as shown in Figure 9:

$$\sum_{k=1}^{n} (\varphi_k + \psi_k) = \Phi \qquad (2b)$$

Calculation of the radii

The system of nonlinear equations determined in the two previous sub-sections is square: the number of equations is the same as the number of unknowns. Since the equations are analytical, the Jacobian matrix of the system can be calculated exactly. Radii fulfilling all the constraints are searched using the

Newton-Raphson method. Note that the value of the radii need to be higher than 0 and lower than π. This constraint is automatically fulfilled using the logarithmic radii as variables. The following initial spherical radii were used for the pictures shown in this paper: *0.24 rad* for the larger circles of each pair, and *0.15 rad* for the smaller. This algorithm converges fairly quickly. Eight iterations are sufficient to generate the trinoid shown in Figure 1.

Construction of the ODCP

These two sets of constraints are sufficient for radii to be compatible with a simply connected ODCP structure. The ODCP is built from the circles as follow:

- First, pairs of circles are placed on two edges of the boundaries of the packing. Only the circle radii and the boundary angles are needed for this purpose.
- The remaining circles are added by propagation from the edges using the orthogonality property and the radii.

4.3 Construction of the discrete Gauss map

The construction of the Gauss map starts with the construction of the circular cones which are tangent to S^2 along the larger node-centered circles of the ODCP. Such cones are shown on the right side of Figure 10.

Prop 1

The apexes of these cones are the vertices of a polyhedral mesh with planar faces and orthotropic edge offset property, i.e. each edge is tangent to either S^2 or tS^2 (a sphere or radius t concentric with S^2).

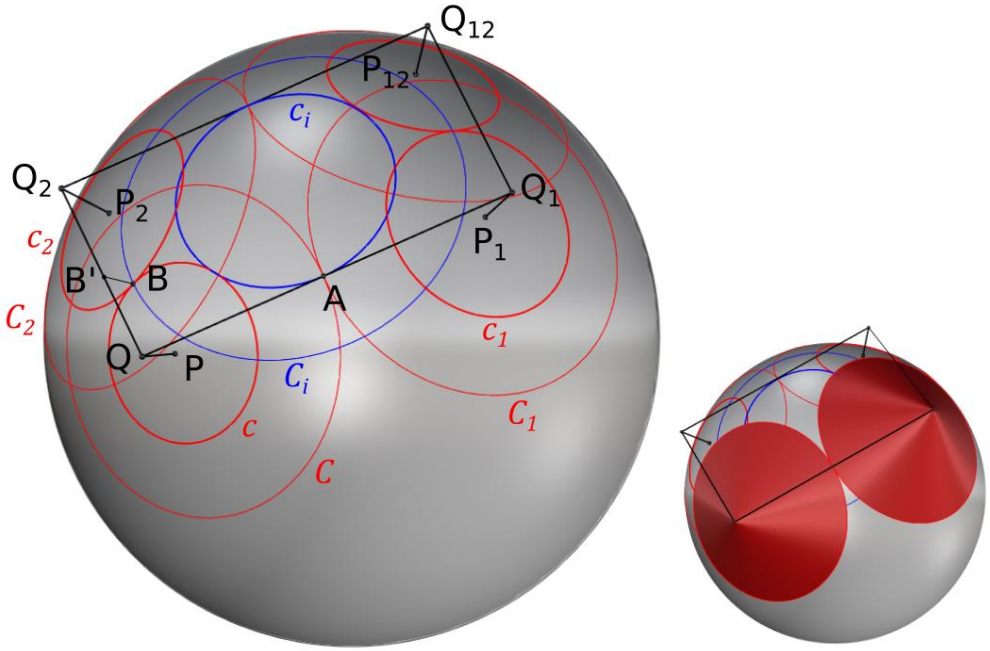

Figure 10: Construction of the Gauss map from the ODCP. Cones used to build the mesh are shown on the right.

Proof:

Starting from an object X of the ODCP, we will call X_1 (resp. X_2) the next object in the direction of higher (resp. lower) curvature – i.e. the direction in which the larger (resp. smaller) circles are tangent.

Let us call (see Figure 10):

- P the center of a node-centered circle of the ODCP ($P \in S^2$) ;
- Q the cone apex corresponding to P ;
- O the center of S^2 ;
- C and c the node-centered circles centered at P, whose spherical radii are respectively R and r (spherical radii are angles in S^2, see Figure 11);
- C_i and c_i the inscribed circles of the spherical face $PP_1P_{12}P_2$.

Q, Q_1 and A are aligned, because the cones centered on P and P_1 are tangent to S^2 at A, and A belongs to the plane OPP_1. Since (QQ_1) and c_i are incident (at A) and since (QQ_1) is tangent to S^2 at A, (QQ_1) and c_i are necessarily coplanar. The same argument can be used to show that (Q_2Q_{12}) and c_i are coplanar. Therefore the quad $QQ_1Q_{12}Q_2$ is planar.

Let us now build the circle c', which is the projection of c onto tS^2, and then build the cones tangent to tS^2 along c'. Q', the apex of this cone belongs to (OP), and its distance to O is (see Figure 11), using Equation (1):

$$OQ' = OB' / \cos r = t / \cos r = 1 / \cos R = OQ$$

Therefore Q' = Q, and we conclude that (QQ_2) and (Q_1Q_{12}) are tangent to tS^2. □

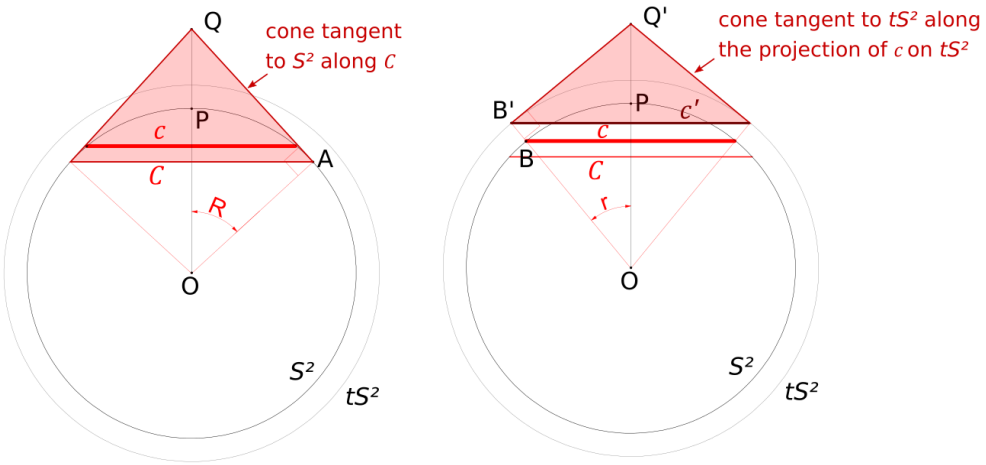

Figure 11 : Tangency of edges with tS^2

5 Reconstruction of the surface from the Gauss map

In this section, we will show how to construct an S-CMC surface from the Gauss map built in Section 4. We start by constructing a double-sphere packing thanks to the underlying ODCP. To each node-centered pair of circles, we associate a pair of spheres centered on the node of the Gauss mesh. Figure 12 shows on the left (resp. right) a section of the double-sphere-packing along the edge of the mesh where the larger (resp. smaller) spheres touch each other:

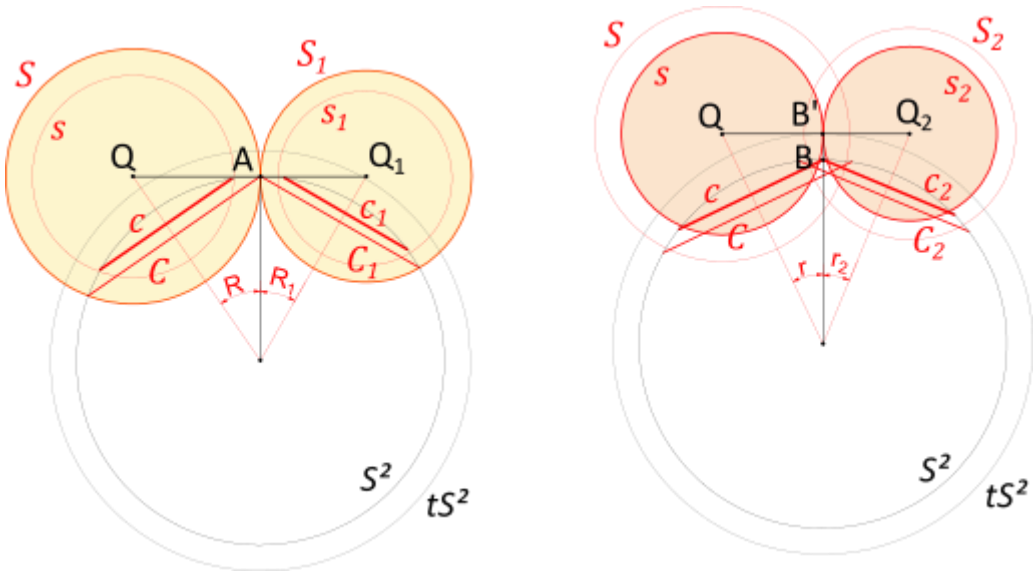

Figure 12 : Double-sphere packing associated with the Gauss map

The radii of the larger and the small spheres are given respectively by:

$$R_S = AQ = \tan(R)$$

$$r_s = B'Q = t * \tan(r)$$

Prop 2

Let *G* be a Gauss map constructed in Section 4. Let *R* and *r* be the radii of the associated double sphere packing. There exist two S-isothermic meshes, M^+ and M^-, which are edgewise parallel to *G*. The radii of the associated spheres are $(R + r)/2$ for M^+, and $(R - r)/2$ for M^-.

Proof:

Figure 13 shows a top view of a face of the Gauss map, with the associated double-spheres. Since the face is closed, we have:

$$(R + R_1)u + (r_1 + r_{12})v_1 - (R_{12} + R_2)u_2 - (r_2 + r)v = 0$$

In which $u = \frac{\overrightarrow{QQ_1}}{QQ_1}$ and $v = \frac{\overrightarrow{QQ_2}}{QQ_2}$

As shown in Figure 13, we can obtain a second sphere packing by switching the direction of tangency of the smaller spheres with that of the larger spheres. This switch can be executed by applying a reflection to each colored quad.

Thanks to the fact that each colored quad has two right angles, the flipped Gauss mesh is parallel to the original one. Therefore, we obtain the following equations, which corresponds to the closure of the quad $\widetilde{Q}\widetilde{Q_1}\widetilde{Q_{12}}\widetilde{Q_2}$:

$$(r + r_1)u + (R_1 + R_{12})v_1 - (r_{12} + r_2)u_2 - (R_2 + R)v = 0$$

As a result, spheres of radius $(R + r)/2$ can be packed in directions parallel to the Gauss mesh:

$$\left(\frac{R + r}{2} + \frac{R_1 + r_1}{2}\right)u + \left(\frac{R_1 + r_1}{2} + \frac{R_{12} + r_{12}}{2}\right)v_1 - \left(\frac{R_{12} + r_{12}}{2} + \frac{R_2 + r_2}{2}\right)u_2 - \left(\frac{R_2 + r_2}{2} + \frac{R + r}{2}\right)v = 0$$

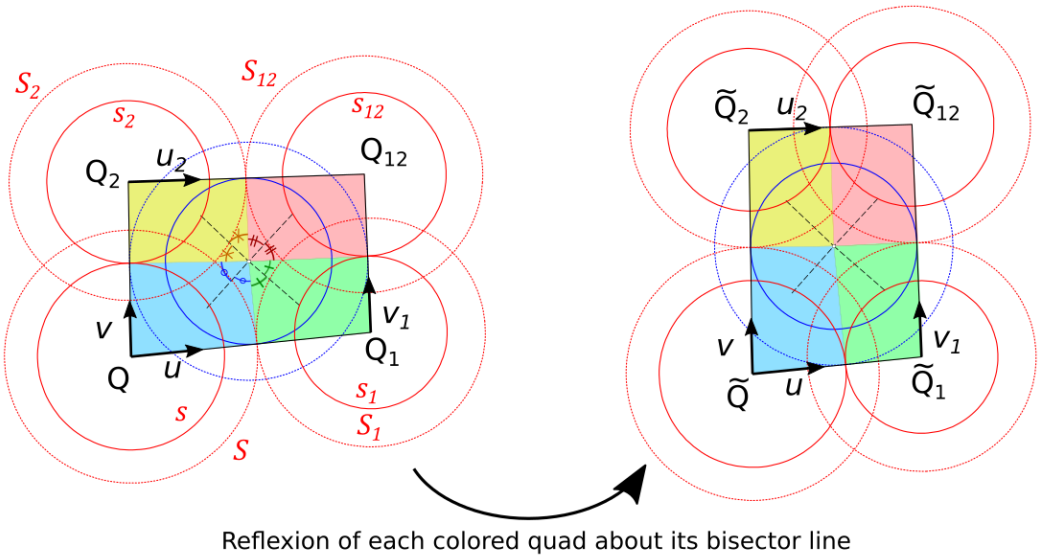

Figure 13 : Change of the direction of the packing of double spheres

This compatibility equation insures that the whole Gauss map can be deformed into an S-isothermic mesh by a Combescure transformation. The edge length modification ratios of this transformation are simply obtained from the sphere radii.

The same result holds for a packing of spheres of radii *(R-r)/2*. □

Prop 3

The S-isothermic meshes M^+ and M^- mentioned in Prop 2 are also S-CMC.

Proof:

Note: For sake of conciseness many of the mathematical concepts used in this proof (such as the Christoffel dual) are not introduced. The reader is advised to browse the paper by Hoffmann (2010) beforehand.

S-CMC meshes are defined as S-isothermic meshes for which the Christoffel dual mesh is also a Darboux transform of the mesh. We start by constructing the mesh $M^* = M^+ + n$ where *n* is the Gauss map and "+" is the sum on vertices. We call C_i the vertices of M^+, C_i^* those of M^*, and A_i the points of tangency of the spheres of M^+.

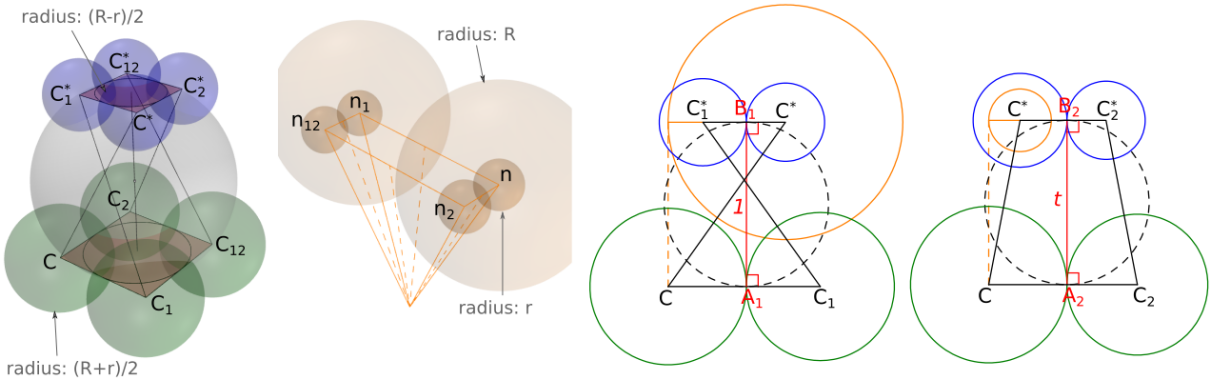

Figure 14 : Construction of the Christoffel dual. From left to right: 3D view of meshes, 3D view of Gauss map (larger spheres centered on n_2 and n_{12} are hidden for clarity), section in higher curvature direction, section in lower curvature direction.

Figure 14 shows the construction in the planes (CC_1C^*) and (CC_2C^*). In each of these planes, we draw a line perpendicular to (CC_i) going through A_i. We call B_i the intersection of this line with $(C^*C_i^*)$. Since edges of the Gauss map *n* are tangent to S^2 and tS^2, $A_1B_1 = 1$ and $A_2B_2 = t$. We note that:

$$C^*B_1 = R - \frac{R+r}{2} = \frac{R-r}{2}$$

$$C^*B_2 = \frac{R+r}{2} - r = \frac{R-r}{2} = C^*B_1$$

Therefore, we can construct a packing of tangent spheres of radii $\frac{R-r}{2}$ centered on vertices of M^*. Since M^* is parallel to M^+, it is also parallel to M^-. As a result, M^* corresponds to the mesh M^-.

The product of the radii of corresponding spheres of M^+ and M^* is:

$$\frac{R+r}{2}\,\frac{R-r}{2} = \frac{R^2-r^2}{4} = \frac{t^2-1^2}{4} = cte \qquad (3)$$

where we use the fact that:

$$CC^{*2} = R^2 + 1 = r^2 + t^2$$

Therefore M^* is the Christoffel dual of M^+.

The circles inscribed in the quads $CC_1C_{12}C_2$ et $C^*C_1^*C_{12}^*C_2^*$ are coaxial. The sphere containing these two circles is orthogonal with the eight spheres centered on each vertex. Therefore, M^* is a Darboux transform of M^+. We can then conclude that M^+ is S-CMC. □

6 Change of curvature

The junctions between zones of positive and negative curvature require a specific treatment. At such a location, the Gauss map of the surface is ''folded''. This section describes how the discrete Gauss map can be folded while keeping the geometric properties described in the previous sections.

6.1 Structure of the Gauss map on a fold

In the model presented in this paper, the curvature is defined on the nodes of the mesh: if a node has a positive (resp. negative) curvature, the associated sphere in the S-CMC mesh has a radius of *(R+r)/2* (resp. *(R-r)/2*). In the cases treated in the previous sections, each face had four nodes with the same curvature sign. As a result, all the circles of the ODCP (and consequently all the spheres of the sphere packing) were tangent on the outside. When a change of curvature occurs, two adjacent smaller circles touch each other on the inside, as shown in Figure 15 :

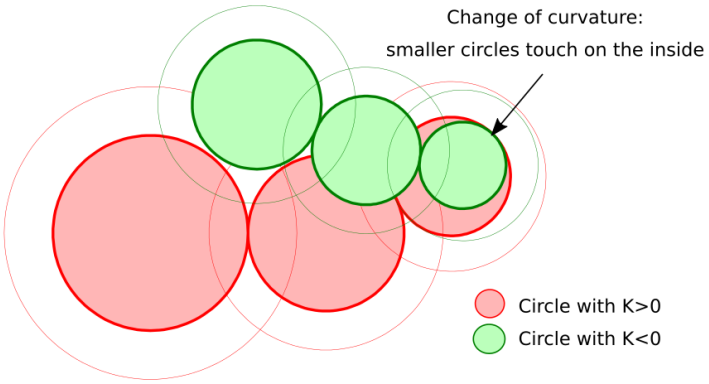

Figure 15 : Change of curvature sign in a line of double-circles of an ODCP of a Gauss mesh

Quads of the Gauss map with nodes of different curvature signs can be classified in the following types, as represented in Figure 16:

- Faces of type A: two nodes have positive curvature, and the two others have negative curvature. The change of curvature occurs when traveling in the direction of low curvature (the direction in which smaller circles are tangent).
- Faces of type B: same as type A, except that the change of curvature occurs when traveling in the direction of higher curvature (the direction in which larger circles are tangent). In that particular case, the inside tangency shown in Figure 15 does not apply.
- Faces of type C: this type is only encountered in highly coarse meshes and will not be treated here.
- Faces of type D: one node has a curvature sign different from the other three.

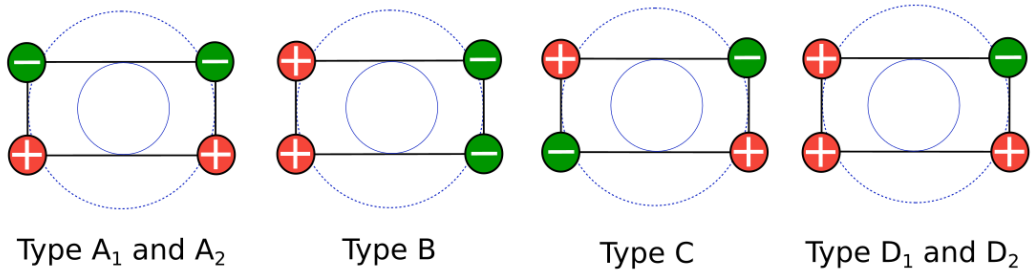

Figure 16: Types of quads with non-uniform node curvature signs

The full tangency pattern for each type of face is shown in Figure 17. For faces of type A and D, it can be noted that, depending on relative size of the adjacent circles, the quad can auto-intersect. Faces of type B always auto-intersect, in the way of a candy wrapping paper. For faces A and D, the tangency of quad edges with tS^2 happens outside of the quad. The types of fold of a quad are analogous to how a rectangle of fabric can be folded, as shown in Figure 18.

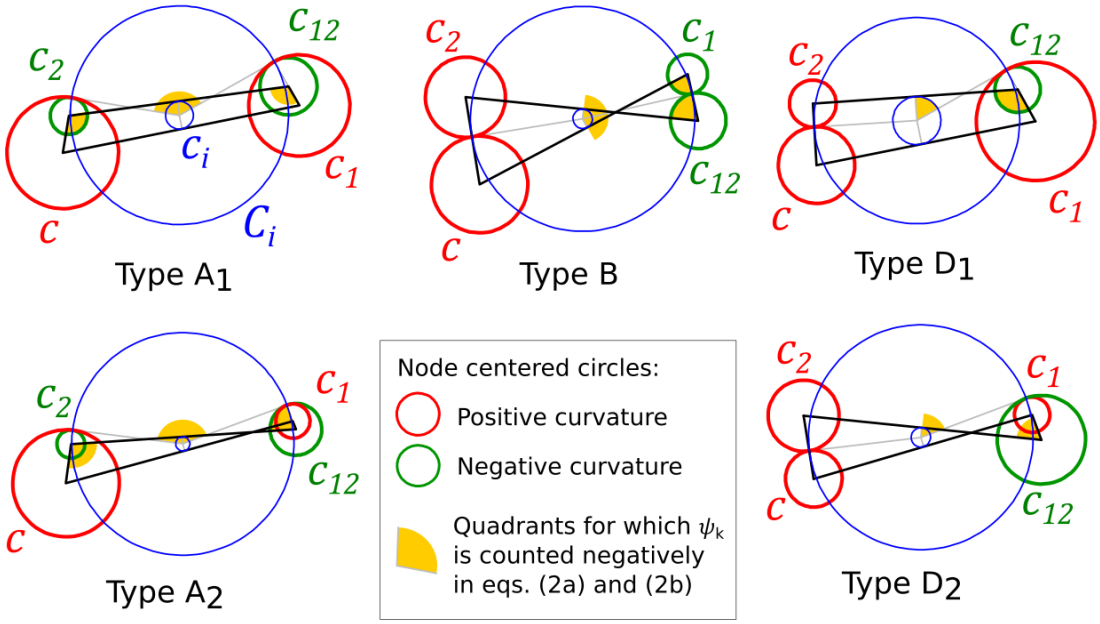

Figure 17: Tangency of circles for the five types of face with a change of curvature sign (larger node centered circles not shown for clarity)

Figure 18: An illustration of the five types of fold with a piece of fabric

6.2 Reconstruction of the surface

Prop 4

Each of the five proposed Gauss map folds can yield a transition part between synclastic and anticlastic portions of a mesh that conserves the S-CMC property.

Proof:

For sake of conciseness, we will only prove the result for faces of type A_1. Looking at one face $QQ_1Q_{12}Q_2$ on Figure 19, we notice that we can pack spheres of radius $(R_i+r_i)/2$ at Q and Q_1 and $(R_i-r_i)/2$ at Q_2 and Q_{12} to form a quad with an inscribed circle:

$$(R+R_1)u+(r_1-r_{12})v_1-(R_{12}+R_2)u_2-(r-r_2)v=0$$

$$(r+r_1)u+(R_1+R_{12})v_1+(r_{12}+r_2)u_2-(R+R_2)v=0$$

$$\Rightarrow \left(\frac{R+r}{2}+\frac{R_1+r_1}{2}\right)u+\left(\frac{R_1+r_1}{2}+\frac{R_{12}-r_{12}}{2}\right)v_1-\left(\frac{R_{12}-r_{12}}{2}+\frac{R_2-r_2}{2}\right)u_2$$
$$-\left(\frac{R_2-r_2}{2}+\frac{R+r}{2}\right)v=0$$

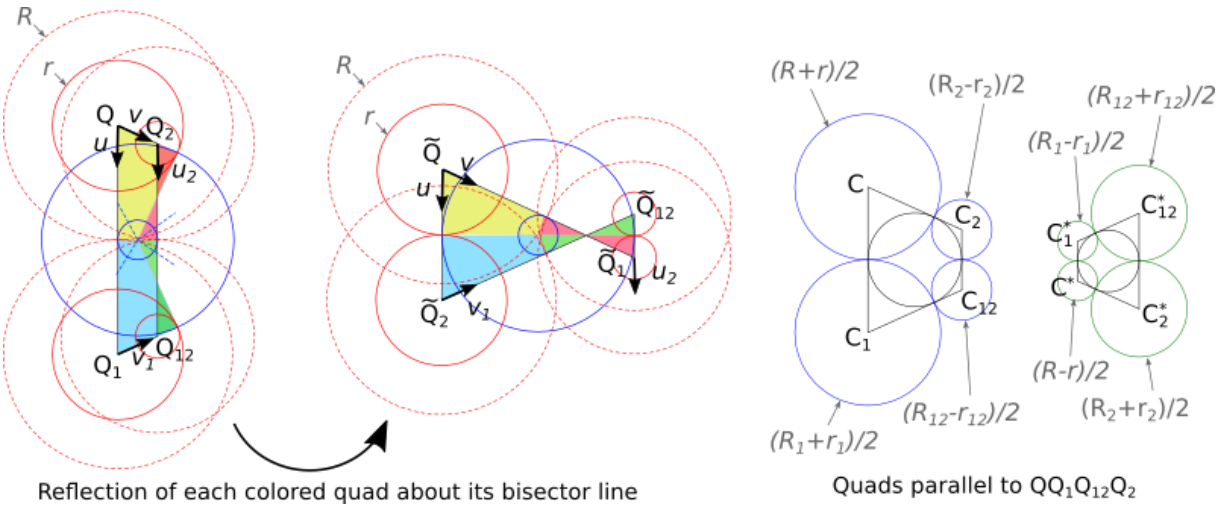

Figure 19 : Construction of faces with inscribed circle from a Gauss face of type A_1 (circle radii are indicated in grey with an arrow)

Note that the same result can be achieved with spheres of radii $(R_i-r_i)/2$ at Q and Q_1 and $(R_i+r_i)/2$ at Q_2 and Q_{12}:

$$-\left(\frac{R-r}{2}+\frac{R_1-r_1}{2}\right)u+\left(\frac{R_1-r_1}{2}+\frac{R_{12}+r_{12}}{2}\right)v_1+\left(\frac{R_{12}+r_{12}}{2}+\frac{R_2+r_2}{2}\right)u_2$$
$$-\left(\frac{R_2+r_2}{2}+\frac{R-r}{2}\right)v=0$$

If we look at a strip of quads (*i.e.* a mesh with only one row) of type A_1, we can now obtain a strip of S-isothermic mesh Str^+. Vertices can be assigned a sphere or radius $(R_i+r_i)/2$ on side of the strip and $(R_i-r_i)/2$ on the other side.

If we now look at $Str^* = Str^+ + n$, the same reasoning as in the proof of prop 3 shows that Str^* is the dual and a Darboux transform of $Str+$. Therefore, $Str+$ is S-CMC. It can thus connect an S-CMC mesh with spheres of radii $(R+r)/2$ (synclastic) to an S-CMC mesh with radii $(R-r)/2$ (anticlastic). Figure 20 shows the connection of the face A_1 with adjacent faces. □

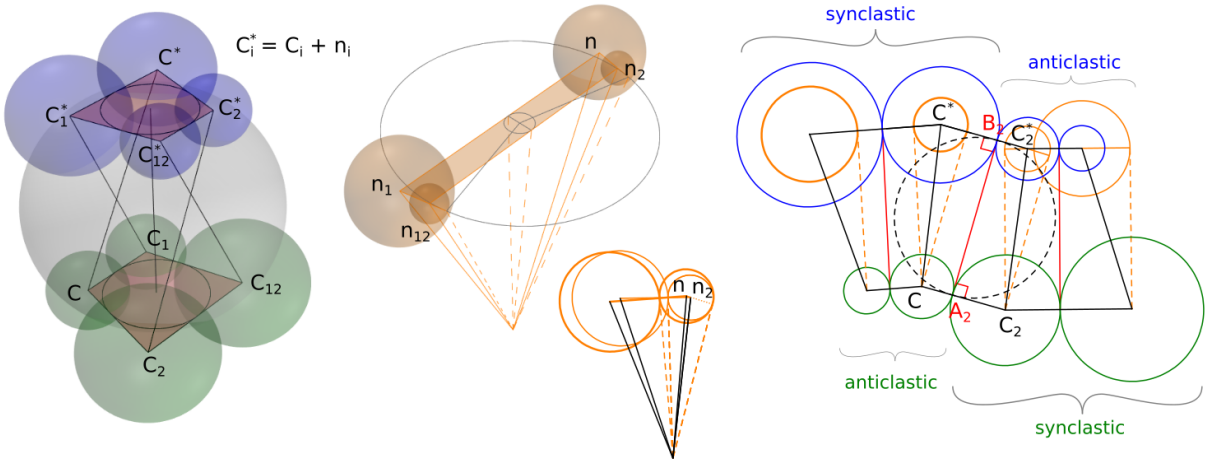

Figure 20 : Arrangement of spheres at a face of type A_1. Left: The face and its dual form a Darboux pair ; Middle: Corresponding Gauss map in 3D and in side view including adjacent faces ; Right: Side view of M and M.*

It can be noted that equations (2a) and (2b) need to be modified on the fold of the Gauss map: the angles ψ_k shall be counted negatively at locations shown on Figure 17. The type of quad is thus a necessary input of the algorithm. The convergence is much less robust when there is a change of curvature.

7 Applications and discussion

Examples

The unduloid is a periodic cylindrical CMC. Although a discrete S-CMC unduloid can be generated rather simply by a so-called elliptic billiard, as explained in Hoffmann (2010), the unduloid shown in Figure 5 was generated with our framework, using as input the analytical equations of the smooth unduloid.

Figure 1 shows an S-CMC version of the trinoid, another well-known CMC surface. Singularities, such as the valence-6 node at the center, can be efficiently handled by the method. The constant *t* for this mesh is 1.004. Therefore, the edge offset in the higher curvature direction is only 0.4% lower than in the lower curvature direction. This fact is particularly interesting considering one major limitation of the edge offset meshes: at locations of a surface where there is a significant difference between the higher and the lower principal curvature, faces are highly elongated. This effect can be observed in some of the work of Pottman *et al* (2007). In the case of this trinoid, we observe that by allowing a slight change between the edge offsets in the two curvature directions, we can obtain faces with an aspect ratio close to one. Furthermore, the difference between the two offsets is low enough to be

considered as a regular edge offset for fabrication purposes. Finally, it is important to note that this S-CMC mesh can fulfill the properties (planarity, offset, etc.) with arbitrary precision.

Figure 21 shows an S-CMC mesh with changing curvature sign. The associated sphere packing is shown on the right. The mesh is generated from a portion of 4-noid, and successive reflections yield the full mesh. The eight-valent nodes could be replaced by planar octagons for improved uniformity of panel sizes.

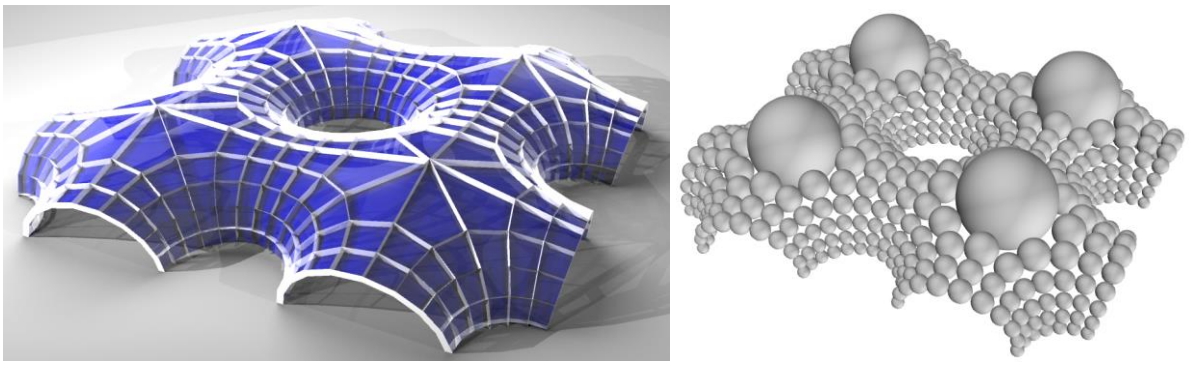

Figure 21 : An S-CMC mesh with changing curvature sign

Figure 22 shows multiple morphologies that can be obtained with a given trinoid combinatorics. The boundaries of the meshes are planar, this simplifies the fabrication of the edge beams. The various shapes are obtained by varying the position and orientation of the boundary planes.

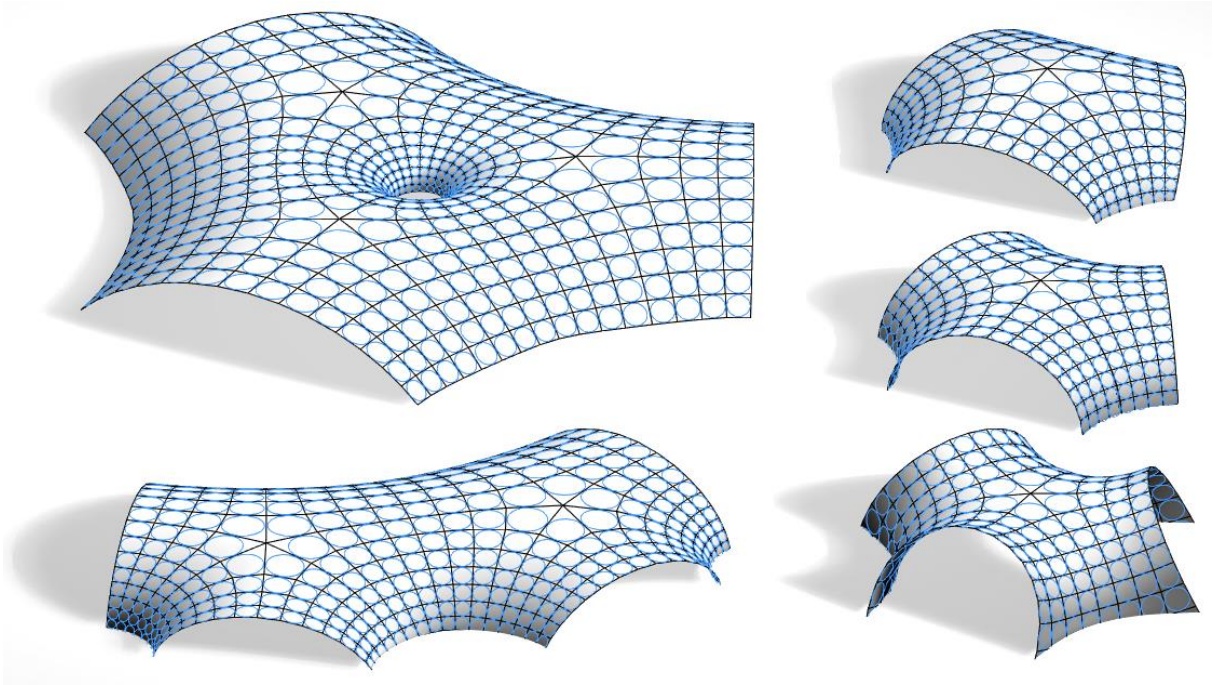

Figure 22 : Several S-CMC trinoids. Left: combining three and two trinoids ; Right: different ways to "inflate" a trinoid

Limitations

The following limitations apply:

- As with other types of meshes with torsion-free nodes, S-CMC meshes can be interpreted as a curvature line network. As such, one cannot choose the orientation of the mesh.
- The final geometry is highly dependent on the combinatorics of the curvature line network. The isothermic condition and the positioning of singularities on umbilics can be difficult to obtain with commercially available software. Furthermore, the network (and therefore the S-

CMC mesh) might need significant refinement when some umbilics are located close to each other.

- In the meshes shown in this paper, boundaries are planar curvature lines. For other types of boundaries, the computation of the boundary angles often requires an optimization loop to approximate the desired smooth surface. This aspect is under development and will be detailed in further publications.
- CMC surfaces that are not simply connected (e.g. surfaces with holes) need periodicity constraints on the top of the ones given in Section 4.2 to ensure proper closing.

Comparison with other generation methods

As a final remark, S-CMCs could also be generated by optimizing directly a mesh. Both vertex positions and vertex normals would then need to be optimized simultaneously. This would make the optimization quite more complex than for circular and conical meshes, for which vertex positions are the only variables. An advantage of such a method would be a stronger control of the boundary, allowed by the ability to "relax" the S-CMC property. Comparatively, our method uses less degrees of freedom, fulfills the S-CMC property exactly and fit boundaries in an approximate manner.

Conclusion

In this paper, we identified the potential of S-CMC meshes for construction-aware design of free-form architectural envelopes. We proposed a method to generate these meshes by discretizing smooth CMCs. We developed a geometric structure that allows the construction of S-CMCs with changing curvature sign. Finally, we demonstrated the morphological potential of S-CMCs on several examples

Acknowledgment

This work is supported by Labex MMCD (http://mmcd.univ-paris-est.fr/), Labex Bezout (http://bezout.univ-paris-est.fr/) and I-SITE GAMES Impulsion project. We warmly thank Tim Hoffmann for inspiring discussions about S-CMC meshes. We would also like to thank Laurent Monasse and Pierre Margerit for their support on numerical and computational aspects and Siavash Ghabezloo for his help with bubble photography.

References

Bach, K. , Burkhard, B. and Otto, F. 1988. "*IL 18. Forming Bubbles*". Institute for Lightweight structures, University of Stuttgart.

Bouaziz, S. , Deuss, M. , Schwartzburg, Y. , Weise, T. and Pauly, M. 2012. "Shape-Up : Shaping Discrete Geometry with Projections." *Eurographics Symposium on Geometry Processing* 31. doi:10.1111/j.1467-8659.2012.03171.x.

Brakke, K. (1992). The Surface Evolver. *Experimental mathematics Volume 1,1992 – Issue2 p141-165*

Bobenko, A. , Hoffmann T. , and Springborn, B. 2006. “Minimal Surfaces from Circle Patterns : Geometry from Combinatorics.” *Annals of Mathematics* 164: 231–64.

Bobenko, A. , and Hoffmann, H. 2016. “S-Conical CMC Surfaces. Towards a Unified Theory of Discrete Surfaces with Constant Mean Curvature.” In *Advances in Discrete Differential Geometry*, 287–308. doi:10.1007/978-3-662-50447-5.

Bobenko, A. and Romon, P. 2017. “Discrete CMC Surfaces in R 3 and Discrete Minimal Surfaces in S 3 : A Discrete Lawson Correspondence.” *Journal of Integrable Systems* 2 (April): 1–18.

Bücking, U. 2007. “Approximation of Conformal Mappings by Circle Patterns and Discrete Minimal Surfaces.” *PhD Diss., Technischen Universität Berlin*.

Gutierrez, C, and Sotomayor, J. 1986. “Principal Lines on Surfaces Immersed with Constant Mean Curvature.” *Transactions of the American Mathematical Society* 293 (February). doi:10.1090/S0002-9947-1986-0816323-5.

Hertrich-Jeromin, U. and Pedit, F. 1997. “Remarks on the Darboux Transform of Isothermic Surfaces.” In *Documenta Mathematica*, 313-333.

Hoffmann, T. 2010. “A Darboux Transformation for Discrete S-Isothermic Surfaces.” *Journal of Math-for-Industry* 2 ((2010B-6)): 157–69.

Oberknappl, B., and Polthier, K. 1997. “An Algorithm for Discrete Constant Mean Curvature Surfaces.” *Visualization and Mathematics*, 141–61.

Pan, H. , Choi Y.-K. , Liu, Y. , Hu, W. , Du, Q. , Polthier, K. , Zhang, C. , and Wang, W. 2012. “Robust Modeling of Constant Mean Curvature Surfaces.” *ACM Transactions on Graphics (TOG)* 31 (4): 11–85. doi:10.1145/2185520.2185581.

Pottmann, H. , Liu, Y. , Wallner, J. , Bobenko, A., and Wang, W. 2007. “Geometry of Multi-Layer Freeform Structures for Architecture.” *ACM Transactions on Graphics* 26 (3): 65. doi:10.1145/1276377.1276458.

Rogers, C., and Schief, W.-K. 2003. “On the Equilibrium of Shell Membranes under Normal Loading. Hidden Integrability.” *Proceedings of the Royal Society of London A: Mathematical, Physical and Engineering Sciences* 459 (2038): 2449–62. doi:10.1098/rspa.2003.1135.

Schoen, R. 1983. “Estimates for Stable Minimal Surfaces in Three Dimensional Manifolds.” In *Seminar on Minimal Submanifolds*, Ann. of Math. Stud. 103, 111–126. Princeton Univ. Press.